Chapter 11
A Map Approach to Stationary Solutions of the DNLS Equation

Ricardo Carretero-González

11.1 Introduction

In this chapter we discuss the well-established map approach for obtaining stationary solutions to the one-dimensional (1D) discrete nonlinear Schrödinger (DNLS) equation. The method relies on casting the ensuing stationary problem in the form of a recurrence relationship that can in turn be cast into a two-dimensional (2D) map [1–5]. Within this description, any orbit for this 2D map will correspond to a steady state solution of the original DNLS equation.

The map approach is extremely useful in finding localized solutions such as bright and dark solitons. As we will see in what follows, this method allows for a global understanding of the types of solutions that are present in the system and their respective bifurcations.

This chapter is structured as follows. In Sect. 11.2 we introduce the map approach to describe steady states for general 1D nonlinear lattices with nearest-neighbor coupling. In Sect. 11.3 we present some of the basic properties of the 2D map generated by the 1D DNLS lattice and how these properties, in turn, translate into properties for the steady-state solutions to the DNLS. We also give an exhaustive account of the possible orbits that can be generated using the map approach. Specifically, we describe in detail the families of extended steady-state solutions (homogeneous, periodic, quasi-periodic, and spatially chaotic) as well as spatially localized steady states (bright and dark solitons and multibreather solutions). In Sect. 11.4 we study the limiting cases of small and large couplings. We briefly describe the bifurcation process that is responsible for the mutual annihilation of localized solutions through a series of bifurcations. For a more detailed account of the bifurcation scenaria for the DNLS using the map approach, see [3].

R. Carretero-González (✉)
Nonlinear Dynamical Systems Group, Computational Science Research Center, and Department of Mathematics and Statistics, San Diego State University, San Diego CA, 92182-7720, USA
e-mail: carreter@sciences.sdsu.edu

P.G. Kevrekidis, *The Discrete Nonlinear Schrödinger Equation*, STMP 232, 221–233, DOI 10.1007/978-3-540-89199-4_11,

11.2 The 2D Map Approach for 1D Nonlinear Lattices

The 2D map approach that we present can be used in general for any 1D nonlinear lattice as long as the coupling between lattice sites is restricted to nearest neighbors. The most common form of such coupling scheme is the discrete Laplacian $\Delta u_n = u_{n-1} - 2u_n + u_{n+1}$. In order to describe the map approach in its more general form, let us consider a generic nonlinear lattice of the form

$$\dot{u}_n = G(u_{n-1}, u_n, u_{n+1}) + F(u_n), \tag{11.1}$$

where G is the nearest-neighbor coupling function and F corresponds to the on-site nonlinearity. The case of the DNLS with the standard cubic nonlinearity is obtained by choosing $G = (\epsilon/i)\Delta$ (Δ will be used to denote the discrete Laplacian) and $F(u) = (\beta/i)|u|^2 u$, where $\epsilon \geq 0$ is the coupling constant and $\beta = \pm 1$ corresponds to defocusing and focusing nonlinearities, respectively. For the map approach to be directly applicable we need to rewrite the steady-state solution of Eq. (11.1) as a recurrence relationship. Therefore, the only requirement for the map approach to work in the general case of the system (11.1) is that the coupling function needs to be invertible with respect to u_{n+1} such that $G(u_{n-1}, u_n, u_{n+1}) = G_0$ can be *explicitly* rewritten as $u_{n+1} = G^{-1}(u_{n-1}, u_n, G_0)$. In particular, this is the case for any coupling function defined as a linear combination of nearest neighbors (which is the case of the discrete Laplacian). For the sake of definitiveness, let us concentrate on the DNLS with cubic nonlinearity but keeping in mind that the technique can be applied in more general scenaria (for example, in [4] and [6] unstaggered and staggered solutions of the cubic-*quintic* DNLS are studied in detail).

Let us then start with the 1D DNLS with cubic on-site nonlinear term

$$i\dot{u}_n = -\epsilon \Delta u_n + \beta |u_n|^2 u_n. \tag{11.2}$$

It can be shown [7] that any steady-state solution of Eq. (11.2) must be obtained by separating space and time as $u_n = \exp(i\Lambda t) v_n$, where Λ is the frequency of the solution, which yields the steady-state equation for the real amplitudes v_n:

$$\Lambda v_n = \epsilon(v_{n-1} - 2v_n + v_{n+1}) - \beta v_n^3. \tag{11.3}$$

It is worth noting at this point that in the 1D case the stationary state is determined, without loss of generality, by the *real* amplitude v_n. In higher dimensions, for topologically charged solutions such as discrete vortices and supervortices in 2D [8–12], discrete diamonds and vortices in 3D [13, 14], and discrete skyrmion-type solutions [15], it is necessary to consider a *complex* steady-state amplitude v_n. Nonetheless, it is crucial to stress that the 2D map approach is only applicable for 1D lattices since the steady-state problem for higher dimensional dynamical lattices cannot be reduced to a recurrence relationship as it is the case (see below) for the 1D lattice.

The steady-state equation described by Eq. (11.3) can now be rewritten as the recurrence relationship

$$v_{n+1} = R(v_n, v_{n-1}) \equiv \frac{1}{\epsilon}\left[(\Lambda + 2\epsilon)v_n - \epsilon v_{n-1} + \beta v_n^3\right], \tag{11.4}$$

which in turn can be cast as the 2D map

$$\begin{pmatrix} v_{n+1} \\ w_{n+1} \end{pmatrix} = M \begin{pmatrix} v_n \\ w_n \end{pmatrix}, \qquad M : \begin{cases} v_{n+1} = R(v_n, w_n) \\ w_{n+1} = v_n \end{cases}, \tag{11.5}$$

where the second equation defines the intermediate variable $w_n \equiv v_{n-1}$. It is important to stress that, by construction, *any* orbit of the 2D map (11.5) will correspond to a steady-state solution of the DNLS (11.2). In particular, any given initial condition $P_0 = (v_0, w_0)^T$ for the 2D map will generate the orbit described by the *doubly* infinite sequence of points $(\ldots, P_{-2}, P_{-1}, P_0, P_1, P_2, \ldots)$ where $P_{n+1} = M(P_n)$ and negative subindexes correspond to backward iterates of the 2D map $[P_{n-1} = M^{-1}(P_n)]$. This 2D orbit will in turn correspond to the steady state $\{\ldots, w_{-2}, w_{-1}, w_0, w_1, w_2, \ldots\}$, where $w_n = [M^n(P_0)]_y$ is the y-coordinate (projection) of the nth iterate of P_0 through M. Alternatively, one could also obtain the steady state as $\{v_n\}_{n=-\infty}^{\infty}$, where $v_n = [M^{n+1}(P_0)]_x$ is the x-coordinate (projection) of the $(n+1)$th iterate of P_0.

It is also important to mention that the 2D map approach, although helpful in describing/finding steady-state solutions of the associated nonlinear lattice, does not give any information about the *stability* of the steady states themselves. This is a consequence of separating time from the steady state where one loses all the temporal information (including stability properties). Nonetheless, the 2D map approach does indicate the *genericity* or parametric/structural stability of certain types of orbits. Specifically, if the type of steady state that is been considered corresponds to a 2D map orbit (including fixed points, periodic orbits, and quasi-periodic orbits) that is isolated (i.e., away in physical and parameter space) from a bifurcation point, then this orbit will still exist in the presence of, small, generic parametric *and* external perturbations. This genericity property might be useful in realistic applications where the presence of (a) small errors in the determination of the parameters of the system and (b) external noise is ubiquitous. Note, however, that if the steady state is unstable to start with, the parametric perturbation will not modify its existence but it will remain unstable.

11.3 Orbit Properties and Diversity in the DNLS

Now that we have established the equivalence between a steady state of the DNLS (11.2) and orbits of the 2D map (11.5), let us discuss the different types of orbits that can be generated using the 2D map approach, their bifurcations and some of their basic properties.

11.3.1 Symmetries and Properties of the Cubic DNLS Steady States

All symmetries and properties inherent to the 2D map (11.5) generate respective symmetries and properties for the steady-state solutions to the DNLS. In particular, for the cubic DNLS (cf. Eq. (11.4)), we have the following symmetries and properties:

(a) The inverse map M^{-1}: $M^{-1}(v_n, w_n)^T = (v_{n-1}, w_{n-1})^T$ is identical to M after exchanging $v \leftrightarrow w$. Therefore any forward orbit of the 2D map will have a symmetric backward orbit that is symmetric with respect to the identity line.
(b) Exchanging $v_n \to (-1)^n v_n$ and $w_n \to (-1)^n w_n$ transforms the 2D map M onto $(-1)^n M$ with $\Lambda \to -\Lambda - 4\epsilon$ and $\beta \to -\beta$. This corresponds to the so-called staggering transformation where every solution to the *focusing* ($\beta = -1$) cubic DNLS has a corresponding solution to the *defocusing* ($\beta = +1$) cubic DNLS with adjacent sites alternating signs (and after a rescaling of the frequency).
(c) The 2D map is area preserving and, as a consequence, the steady-state solutions to the DNLS have the following properties. (i) Linear centers of the 2D map are also nonlinear centers and thus there will be periodic and quasi-periodic orbits around (linearly) neutrally stable fixed points. These 2D map orbits correspond, respectively, to spatially periodic and quasi-periodic steady state solutions to the DNLS (see below). (ii) Saddle fixed points of the 2D map will have stable and unstable manifold with the same exponential rates of convergence. Thus, localized steady state solutions of the DNLS will have symmetric tails at $n \to \pm\infty$.

11.3.2 Homogeneous, Periodic, Modulated, and Spatially Chaotic Steady States

In this section we concentrate on describing steady states that are spatially extended (i.e., not localized in space). These correspond to (a) fixed points, (b) periodic orbits, (c) quasi-periodic orbits, and (d) chaotic orbits of the 2D map M.

11.3.2.1 Homogeneous Steady States

The most straightforward orbit that can be described by the 2D map approach is a fixed point. Suppose that $P^* = (v^*, w^*)^T$ is a fixed point of M, namely $M(P^*) = P^*$. This trivial orbit generates the *homogeneous* steady solution $v_n = v^*$. Note that, by construction, all fixed points of M must satisfy $v^* = w^*$. For the DNLS case under consideration, the 2D map fixed point equation $(\Lambda + \beta v^2)v = 0$ has three fixed points $v^* = \{0, \pm\sqrt{-\Lambda/\beta}\}$, that in turn correspond to the two spatially homogeneous solutions $u_n(t) = 0$ and $u_n(t) = \sqrt{-\Lambda/\beta}\, \exp(i\Lambda t)$.

11.3.2.2 Periodic Steady States

Let us now consider a periodic orbit of the 2D map. Suppose that $\{P_0, P_1, ..., P_{p-1}\}$ is a period-p orbit of M (i.e., $M(P_{p-1}) = P_0$). This periodic orbit for M will generate a *spatially periodic* steady-state solution for the DNLS, where $v_n = [P_{n \bmod(p)}]_y$. A particular case of this spatially periodic steady state stems from period-2 orbits $\{T_0, T_1\}$. There are at most three such period-2 solutions depending on the $(\epsilon, \Lambda, \beta)$-parameter values. One of these solutions has the form $T_0 = -T_1 = (+a, -a)^T$ where $a = \sqrt{-(\Lambda + 4\epsilon)/\beta}$. This symmetric period-2 orbit is a consequence of the symmetry of the 2D map under consideration where the transformations $v \leftrightarrow -v$ and $w \leftrightarrow -w$ leave the equations invariant. This symmetric period-2 orbit generates an oscillatory steady-state profile of the form $v_n = (..., -a, +a, -a, +a, ...)$. In general a period-$p$ orbit of the 2D map generates an spatially periodic steady state with spatial wavelength (period) of p.

11.3.2.3 Quasi-Periodic Steady States

An interesting steady-state solution is generated when one considers quasi-periodic solutions of the 2D map. For example, the origin is a nonlinear center for $-4\epsilon < \Lambda < 0$ in both the focusing and defocusing case. Around this center point the 2D map exhibits an infinite family of quasi-periodic solutions rotating about the origin (cf. Fig. 11.1). These 2D map orbits correspond to steady-state modulated waves about the fixed point (in this case the origin) for the DNLS. An example of such an orbit is depicted in Fig. 11.1. In the left panel of the figure we depict with circles the quasi-periodic orbit around the origin, while in the right panel we depict (also with circles) its corresponding steady-state solution to the DNLS. The spatial periodicity of these modulated waves is approximately determined by the argument of the eigenvalues of the Jacobian at the fixed point.

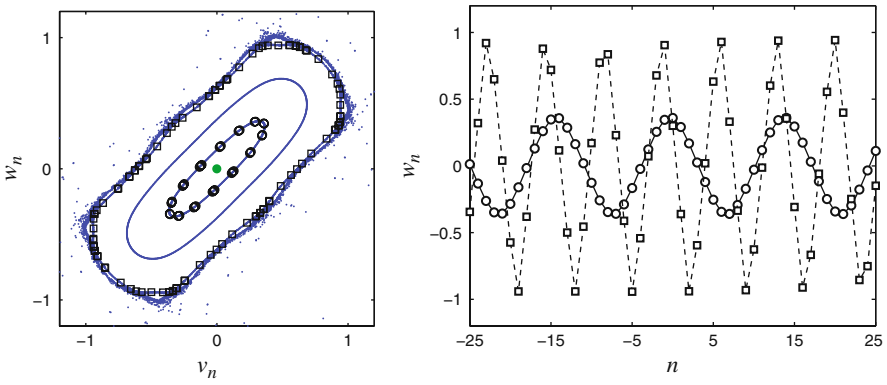

Fig. 11.1 Periodic, quasi-periodic and chaotic orbits of the 2D map (*left*). The *right panel* depicts the corresponding steady-state solutions to the DNLS. Circles (*squares*) correspond to a quasi-periodic (chaotic) orbit. Parameter values correspond to: $\Lambda = -0.1$, $\beta = -1$, and $\epsilon = 1$

11.3.2.4 Spatially Chaotic Steady States

As a last example of a non-localized steady state let us consider the next level of complexity for a 2D orbit: a chaotic orbit. Chaotic orbits will be a common occurrence in nonlinear maps. For the case under consideration, the 2D map induced by the DNLS becomes chaotic close to the separatrix between higher periodic orbits. In Fig. 11.1 we depict such a chaotic region around the separatrix of a pair of period-7 orbits (see outer orbits). Such a chaotic orbit naturally generates a steady-state solution (see squares in the right panel) that resembles a period-7 orbit that is chaotically modulated. It is important to mention that, typically, these chaotic orbits exhibit "stickiness" close to the separatrix (see [16] and references therein for more details on chaotic transport) and thus will stay close to a periodic orbit for some time. However, the chaotic orbit is eventually expelled (both in forward and backward time) and therefore the steady state becomes unbounded at $n \to \pm\infty$. See [17] for a discussion of the relationship between these chaotic orbits and the transmission properties in nonlinear Schrödinger-type lattices.

11.3.3 Spatially Localized Solutions: Solitons and Multibreathers

Undoubtedly, the most interesting steady-state solutions are generated by homoclinic and heteroclinic orbits of the 2D map. These orbits correspond, respectively, to *bright* and *dark* solitons of the DNLS.

11.3.3.1 Homoclinic Orbits

Let us concentrate our attention on homoclinic orbits emanating from the origin. A homoclinic orbit corresponds to an orbit that connects, in forward and backward time, a fixed point with itself. In turn, this corresponds to a non-trivial steady-state solution that decays to the fixed point for $n \to \pm\infty$. This is the so-called *bright soliton* solution. A sufficient condition for the existence of a homoclinic orbit for a 2D map is that the stable (W^s) and unstable (W^u) manifolds of the fixed point intersect. Thus, a necessary condition for the existence of these manifolds is that the fixed point must be a saddle. This latter condition, in turn, translates into a necessary (but not sufficient) condition on the parameters of the system. For example, in the $\Lambda < 0$ case, one needs a coupling constants $\epsilon < -\Lambda/4$ to ensure the origin is a saddle point (for $\Lambda > 0$ the origin is always a saddle point). It is important to stress that the existence of a saddle does not guarantee the existence of a homoclinic connection since the stable and unstable manifolds might not intersect at all. It is possible to formally establish the existence of homoclinic orbits of nearly integrable 2D maps through the Mel'nikov approach [18]. This method has been successfully applied to the single DNLS chain [1] as well as to systems of coupled DNLS equations [19] by means of a higher dimensional Mel'nikov approach [20]. Another approach to establish the existence of the homoclinic orbit is to expand them in a power series using a center manifold reduction [1, 7, 21, 22]. This has the

advantage that one is able to extract an approximation for the homoclinic orbits and thus be able to approximate their bifurcations [23]. See [21] for a comprehensive list of different techniques to approximate the homoclinic connections arising from the DNLS system.

Any intersection between the stable and unstable manifolds (a so-called homoclinic point) will generate a localized steady-state solution for the DNLS. Generically, the stable and unstable manifolds cross transversally giving rise to a so-called homoclinic tangle (see left panel of Fig. 11.2 for a typical example). The transversality of the intersection of the manifolds establishes the *parametric* stability for the existence of homoclinic points and thus localized solutions. This property is extremely important for applications since it guarantees that, despite inaccuracies in the model parameters and external perturbations, localized solutions will still survive. This, for example, allows for *approximate* dynamical reductions to the interactions of continuous chains of bright solitons to be able to perform localized oscillations [24]. Two examples of soliton solutions generated by a homoclinic point of the focusing ($\beta = -1$) 2D map are depicted in Fig. 11.2 and they correspond to *bond-centered* (circles) and *site-centered* (squares) solutions. These two families are generated by the odd and even crossing of the stable and unstable manifolds starting at the points labeled by the points Q_0 and P_0 in the left panel. In general, the 2D map approach not only establishes the existence of bright soliton solutions (as well as dark soliton solutions, see below) but also determines their decay rate. Specifically, the eigenvalues $\lambda_\pm$ ($\lambda_- < 1 < \lambda_+$) for the saddle fixed point supporting the homoclinic orbit (the origin in the case under consideration) determine the *exponential* decay $\lambda_-^{|n|} = \lambda_+^{-|n|}$ for $n \to \pm\infty$ ($\lambda_- = \lambda_+^{-1}$ is a consequence of the

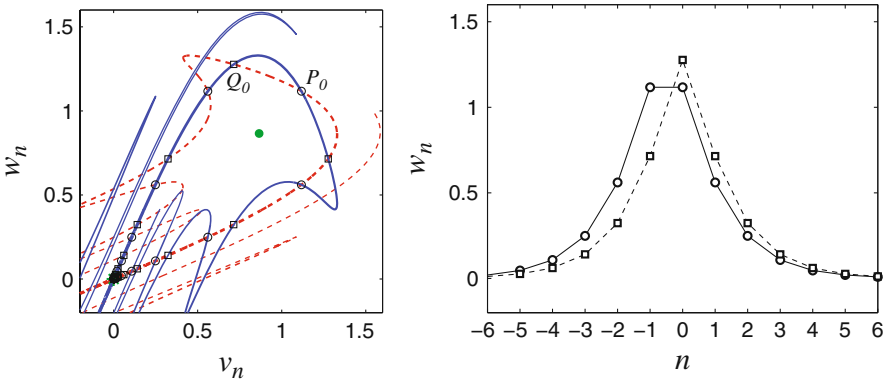

Fig. 11.2 Homoclinic connection of the 2D map (*left*). Stable and unstable manifolds are depicted by *solid* and *dashed lines*, respectively. The *right panel* depicts the corresponding *bright soliton* steady-state solutions to the DNLS. *Circles* (*squares*) correspond to a bond (site) centered bright soliton solution generated by the initial condition depicted in the *left panel* by P_0 (Q_0). Parameter values correspond to: $\Lambda = 0.75$, $\beta = -1$, and $\epsilon = 1$

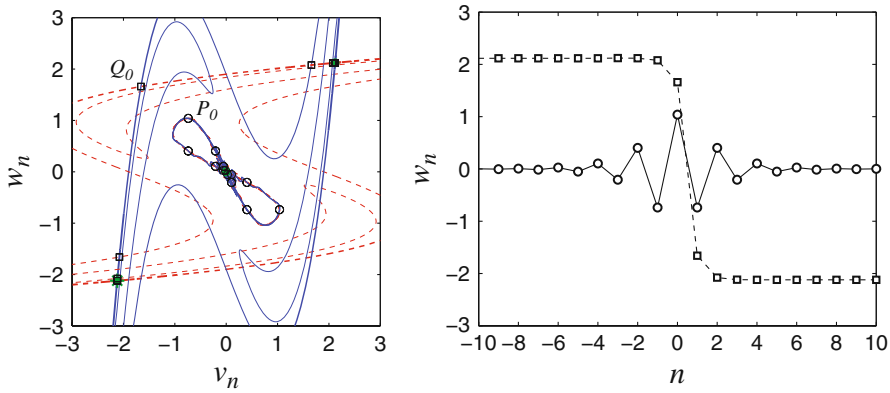

Fig. 11.3 Homoclinic and heteroclinic connections of the 2D map (*left*). Stable and unstable manifolds are depicted by *solid* and *dashed lines*, respectively. The *right panel* depicts the corresponding *dark soliton* (*squares*) and staggered *bright soliton* (*circles*) steady state solutions to the DNLS generated by the initial conditions depicted in the *left panel* by Q_0 and P_0, respectively. Parameter values correspond to: $\Lambda = -4.5$, $\beta = 1$, and $\epsilon = 1$

properties described in Sect. 11.3.1). In our case the eigenvalues at the origin are given by $2\epsilon\lambda_{\pm} = \Lambda + 2\epsilon \pm \sqrt{\Lambda(\Lambda + 4\epsilon)}$.

The staggering transformation generated by the symmetry described in Sect. 11.3.1.(b) establishes the existence of a staggered companion to the above described bright soliton. In Fig. 11.3 we depict with circles such a staggered bright soliton emanating from the initial condition labeled with P_0 in the left panel. The decaying properties for the staggered bright soliton are the same as for its unstaggered sibling.

11.3.3.2 Heteroclinic Orbits

Instead of considering connections involving a single fixed point, consider the stable manifold $W^s(x_1^*)$ emanating from the fixed point x_1^* and the unstable manifold $W^u(x_2^*)$ emanating from the fixed point x_2^* ($x_1^* \neq x_2^*$). If these manifolds intersect then it is possible to induce an orbit that connects, in forward time, x_1^* with, in backward time, x_2^*. This is a so-called *heteroclinic* connection and it corresponds to a steady state that connects to distinct homogeneous steady states (x_1^* and x_2^*), namely a *dark soliton* (or front).

Two examples of dark solitons generated by heteroclinic orbits of the 2D map are depicted in Figs. 11.4 and 11.3. Figure 11.4 depicts a dark soliton in the focusing case which has staggered tails, while Fig. 11.3 depicts (see orbit depicted with squares emanating from the initial condition labeled by Q_0) a standard dark soliton for the defocusing case.

The decaying properties for the tails of the dark soliton can be obtained, as in the case of the bright soliton, by the appropriate eigenvalues of the fixed points supporting the solution.

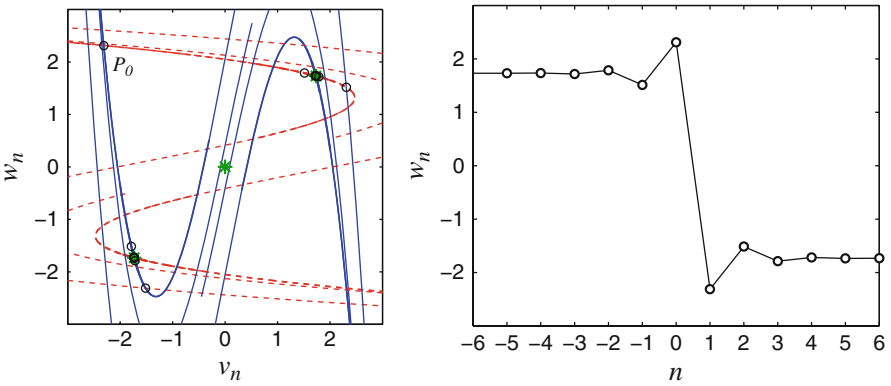

Fig. 11.4 Heteroclinic connection of the 2D map (*left*). Stable and unstable manifolds are depicted by *solid* and *dashed lines*, respectively. The *right panel* depicts the corresponding staggered *dark soliton* steady-state solution to the DNLS generated by the initial condition depicted in the *left panel* by P_0. Parameter values correspond to: $\Lambda = 3$, $\beta = -1$, and $\epsilon = 1$

11.3.3.3 Multibreathers

By following higher order intersections of the homoclinic connections it is possible to construct localized solutions with more than one localized hump [2, 3]. These solutions are usually referred to as *multibreathers*. In Fig. 11.5 we depict three examples of *bright* multibreathers for the same parameters but starting at different intersections on the homoclinic tangle. For a detailed classification of these multibreather solutions see [2] and [3]. Naturally, multibreather solutions are also possible in the defocusing case in the form of dark multisolitons (several contiguous

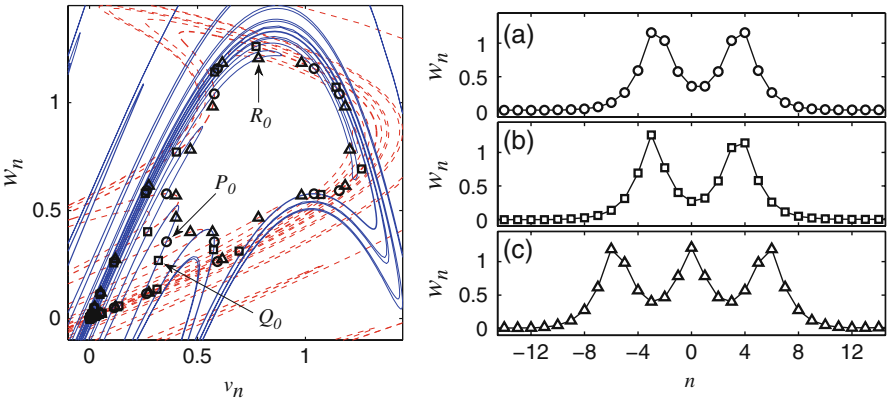

Fig. 11.5 Higher order homoclinic connections corresponding to multibreather solutions. The three multibreather solutions correspond to: (**a**) symmetric two-hump multibreather generated by the initial condition P_0 (see *circles*), (**b**) asymmetric two-hump multibreather generated by the initial condition Q_0 (see *squares*), and (**c**) three-hump multibreather generated by the initial condition R_0 (see *triangles*). Parameter values correspond to: $\Lambda = 0.75$, $\beta = -1$, and $\epsilon = 1$

troughs asymptotic to the constant homogeneous steady-state background) [25, 26]. It is worth mentioning that all the multibreather structures described herein are genuinely discrete solutions and are not related to the multisoliton solutions of the continuous nonlinear Schrödinger equation that can be generated from the single soliton solution by using the inverse scattering theory [27].

11.4 Bifurcations: The Road from the Anti-Continuous to the Continuous Limit

One of the most appealing aspects of the map approach to study steady states of nonlinear lattices is not only the elucidation of the extremely rich variety of structures that can be described but, perhaps more importantly, its usefulness in fully characterizing their bifurcations. The idea is to start at the so-called anti-continuous [28] (uncoupled) limit, $\epsilon = 0$, where any solution $v_n \in \{0, \pm\sqrt{-\Lambda/\beta}\}$ is valid. It is known that *all* possible solutions for $\epsilon = 0$ can be continued to *finite* coupling $\epsilon^* > 0$ [28]. In fact, several works have been devoted to finding bounds for ϵ^* (threshold for coupling below which *any* solution can be found) and they range from $\epsilon^* > 1/(10 + 4\sqrt{2}) \approx 0.0639$ to $\epsilon^* > (3\sqrt{3} - 1)/52 = 0.0807$ [3, 7, 29]. In terms of the 2D map description, the existence of any solution $v_n \in \{0, \pm\sqrt{-\Lambda/\beta}\}$ is a consequence of the fractal structure of the homoclinic tangle for small coupling. In fact, for small ϵ the homoclinic tangles tend to accumulate close to the basic nine points (x, y) with $x, y \in \{0, \pm\sqrt{-\Lambda/\beta}\}$ allowing orbits consisting of any combination of states $v_n \approx \{0, \pm\sqrt{-\Lambda/\beta}\}$ to be possible [3]. This effect can be clearly seen in panel (a) of Fig. 11.6 that corresponds to a very weak coupling $\epsilon = 0.05$ that is below the critical coupling ϵ^* and thus any orbit connecting any possible combination of neighboring basic points is valid.

As the coupling parameter ϵ is increased from the anti-continuous limit, solutions start to dissappear through mutual collisions in saddle node and pitchfork bifurcations. A detailed description of this scenario pertaining to the DNLS can be found in [3]. This work was in turn inspired by a similar analysis performed on the Hénon map [30]. In both [30] and [3] it is conjectured (the so-called no-bubbles-conjecture)

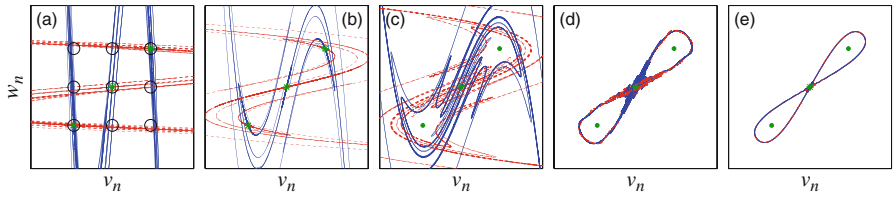

Fig. 11.6 Homoclinic tangle progression as the coupling parameter is increased from the anti-continuous limit toward the continuous limit. The coupling for each panel corresponds, from *left to right*, to $\epsilon = 0.05$, 0.2, 0.6, 1, and 1.5. In panel (**a**) the nine *black circles* correspond to the areas of the 2D map points giving rise to any possible combination $v_n \approx \{0, \pm\sqrt{-\Lambda/\beta}\}$ close to the anti-continuous limit. The other parameter values correspond to: $\Lambda = 0.75$ and $\beta = -1$

that, as the coupling ϵ grows, *only* annihilation of solutions (through saddle node and pitchfork bifurcations) occurs and that no new solutions emerge. In Fig. 11.6 we show the progression of the homoclinic tangle of the origin as the coupling parameter is increased from the anti-continuous limit toward the continuous limit. As it is clearly suggested by the figure, the amount of crossings between the different stable/unstable manifolds is greatly reduced as ϵ is increased. The disappearance of these crossings is accounted by a series of saddle node and pitchfork bifurcations – the saddle node being the most common one. By following the number of different possible homoclinic connections as the coupling is increased one would obtain a Devil (fractal) staircase [31–33] as it is evidenced in Fig. 14 of [3].

In the limit $\epsilon \to \infty$ (the continuous limit), the homoclinic tangle of the origin gets thinner and asymptotically tends towards a *simple* homoclinic connection where the stable and unstable manifolds coincide exactly and correspond to a simple loop as it can be observed from panel (e) of Fig. 11.6. In this continuous limit both, the bond-centered and the site-centered solutions, coalesce into the bright soliton solution to the standard *continuum* nonlinear Schrödinger equation.

11.5 Summary and Future Challenges

In this chapter we presented a review of the so-called map approach whereby the steady-state problem for general nonlinear dynamical lattices, with nearest-neighbor coupling, can be cast as a second-order recurrence equation that, in turn, generates a 2D map. Within this framework, *any* orbit of this 2D map generates a corresponding steady-state solution for the nonlinear lattice. Concentrating on the 2D map generated by the DNLS equation, we first described some generic properties of the steady solutions that are straightforward consequences of the underlying symmetries of the 2D map. Then, we comprehensively studied the diversity of DNLS steady-state solutions that can be generated using this map approach. We partition the possible solutions into spatially extended and localized steady states. Spatially extended states correspond to homogeneous, periodic, modulated, and spatially chaotic steady states of the DNLS and are generated, respectively, by fixed points, periodic orbits, quasi-periodic orbits, and chaotic orbits of the 2D map. The more interesting case of spatially localized steady states is generated by homoclinic or heteroclinic connections of the 2D map that in turn generate, respectively, bright and dark soliton steady-state solutions of the DNLS. We also elaborated on the staggered (oscillating) and multibreather variants thereof. We also briefly described the bifurcation road whereby the extremely rich diversity of solutions generated at the anti-continuum limit (zero coupling) is reduced through a series of saddle node and pitchfork bifurcations to a single solution (the standard bright or dark soliton) at the continuum limit.

Some future challenges related to the map approach would include the corroboration of the the so-called no-bubbles-conjecture, originally put forward by Sterling et al. for the Hénon map [30] and then re-stated for the DNLS 2D map by Alfimov

et al. [3], whereby it is noted that as the coupling parameter is increased only *annihilation* of solutions occurs (through saddle node and pitchfork bifurcations) and thus no "birth" of new solutions may occur. Another topic that has not yet been fully explored is the use of the Mel'nikov approach for higher dimensional maps [20, 34–36] for more complex coupling schemes. In particular, this higher dimensional Mel'nikov approach has been successfully applied to a 1D nonlinear double Ablowitz–Ladik chain [37, 38] (see also Sect. 2.1 in Chap. 2) in [39]. It would be interesting to explore this higher dimensional approach in 1D lattices with higher order neighboring couplings (i.e., not only nearest neighbors) that will naturally generate higher order recurrence relationships between successive lattice sites and therefore higher dimensional maps. Finally, the direct application of the map approach for higher dimensional lattices is not possible because the recurrence relationship equivalent to Eq. (11.4) would involve two and three indices for the 2D and 3D cases, respectively. Nonetheless, it should be in principle possible to treat, for example, a 2D lattice chain as an infinite array of 1D coupled chains and apply the higher dimensional Mel'nikov approach mentioned above for the double Ablowitz–Ladik chain [39]. However, such a scheme is anticipated to be extremely cumbersome and involve complicated numerical methods to evaluate the Mel'nikov approach in high dimensions.

References

1. Hennig, D., Rasmussen, K.Ø., Gabriel, H., Bülow, A.: Phys. Rev. E **54**, 5788 (1996) 221, 226
2. Bountis, T., Capel, H.W., Kollmann, M., Ross, J.C., Bergamin, J.M., van der Weele, J.P.: Phys. Lett. A **268**, 50 (2000) 221, 229
3. Alfimov, G.L., Brazhnyi, V.A., Konotop, V.V.: Physica D **194**, 127 (2004) 221, 229, 230, 231, 232
4. Carretero-Gonzáles, R., Talley, J.D., Chong, C., Malomed, B.A.: Physica D **216**, 77 (2006) 221, 222
5. Qin, W.X., Xiao, X.: Nonlinearity **20** 2305 (2007) 221
6. Maluckov, A., Hadžievski, L., Malomed, B.A.: Phys. Rev. E **77**, 036604 (2008) 222
7. Hennig, D., Tsironis, G.P.: Phys. Rep. **307** 333 (1999) 222, 226, 230
8. Malomed, B.A., Kevrekidis, P.G.: Phys. Rev. E **64**, 026601 (2001) 222
9. Kevrekidis, P.G., Malomed, B.A., Chen, Z., Frantzeskakis, D.J.: Phys. Rev. E **70**, 056612 (2004) 222
10. Sakaguchi, H., Malomed, B.A.: Europhys. Lett. **72**, 698 (2005) 222
11. Neshev, D.N., Alexander, T.J., Ostrovskaya, E.A., Kivshar, Yu.S., Martin, H., Makasyuk, I., Chen, Z.: Phys. Rev. Lett. **92**, 123903 (2004) 222
12. Fleischer, J.W., Bartal, G., Cohen, O., Manela, O., Segev, M., Hudock, J., Christodoulides, D.N.: Phys. Rev. Lett. **92**, 123904 (2004) 222
13. Kevrekidis, P.G., Malomed, B.A., Frantzeskakis, D.J., Carretero-González, R.: Phys. Rev. Lett. **93**, 080403 (2004) 222
14. Carretero-González, R., Kevrekidis, P.G., Malomed, B.A., Frantzeskakis, D.J.: Phys. Rev. Lett. **94**, 203901 (2005) 222
15. Kevrekidis, P.G., Carretero-González, R., Frantzeskakis, D.J., Malomed, B.A., Diakonos, F.K.: Phys. Rev. E **75**, 026603 (2007) 222
16. Balasuriya, S.: Physica D, **202**, 155 (2005) 226
17. Hennig, D., Sun, N.G., Gabriel, H., Tsironis, P.: Phys. Rev. E **52**, 255 (1995) 226
18. Glasser, M.L., Papageorgiou, V.G., Bountis, T.C.: SIAM J. Appl. Math. **49**, 692 (1989) 226
19. Kollmann, M., Bountis, T.: Physica D **113**, 397 (1998) 226

20. Bountis, T., Goriely, A., Kollmann, M.: Phys. Lett. A **206**, 38 (1995) 226, 232
21. James, G., Sánchez-Rey, B., Cuevas, J.: Rev. Math. Phys. **21**, 1 (2009) 226, 227
22. Cuevas, J., James, G., Malomed, B.A., Kevrekidis, P.G., Sánchez-Rey, B.: J. Nonlinear Math. Phys. **15**, 134 (2008) 226
23. Palmero, F., Carretero-González, R., Cuevas, J., Kevrekidis, P.G., Królikowski, W.: Phys. Rev. E **77** 036614 (2008) 227
24. Carretero-González, R., Promislow, K.: Phys. Rev. A **66**, 033610 (2002). 227
25. Susanto, H., Johansson, M.: Phys. Rev. E **72**, 016605 (2005) 230
26. Pelinovsky, D.E., Kevrekidis, P.G.: J. Phys. A: Math. Theor. **41** 185206 (2008) 230
27. Debnath, L.: Nonlinear Partial Differential Equations for Scientists and Engineers. Birkhäuser Boston, (2005) 230
28. MacKay, R.S., Aubry, S.: Nonlinearity **7**, 1623 (1994) 230
29. Dullin, H.R., Meiss, J.D.: Physica D **143**, 265 (2000) 230
30. Sterling, D., Dullin, H.R., Meiss, J.D.: Physica D **134**, 153 (1999) 230, 231
31. Bak, P.: Phys. Today **12** 38 (1986) 231
32. Schroeder, M.: Fractals, Chaos, Power Laws. W.H. Freeman and Company, New York 1991. Chap. 7 231
33. Carretero-González, R., Arrowsmith, D.K., Vivaldi, F.: Physica D **103** 381 (1997) 231
34. Palmer, J.K.: J. Diff. Eqns. **55**, 225 (1984) 232
35. Chow, S.N., Hale, J.K., Mallet-Paret, J.: J. Diff. Eqns. **37**, 351 (1980) 232
36. Chow, S.N., Yamashita, M.: Nonlinear Equations in the Applied Sciences. Academic, New York, (1992) 232
37. Ablowitz, M.J., Ladik, J.F.: J. Math. Phys. **16**, 598 (1975) 232
38. Ablowitz, M.J., Ladik, J.F.: J. Math. Phys. **17**, 1011 (1976) 232
39. Bülow, A., Hennig, D., Gabriel, H.: Phys. Rev. E **59**, 2380 (1999) 232